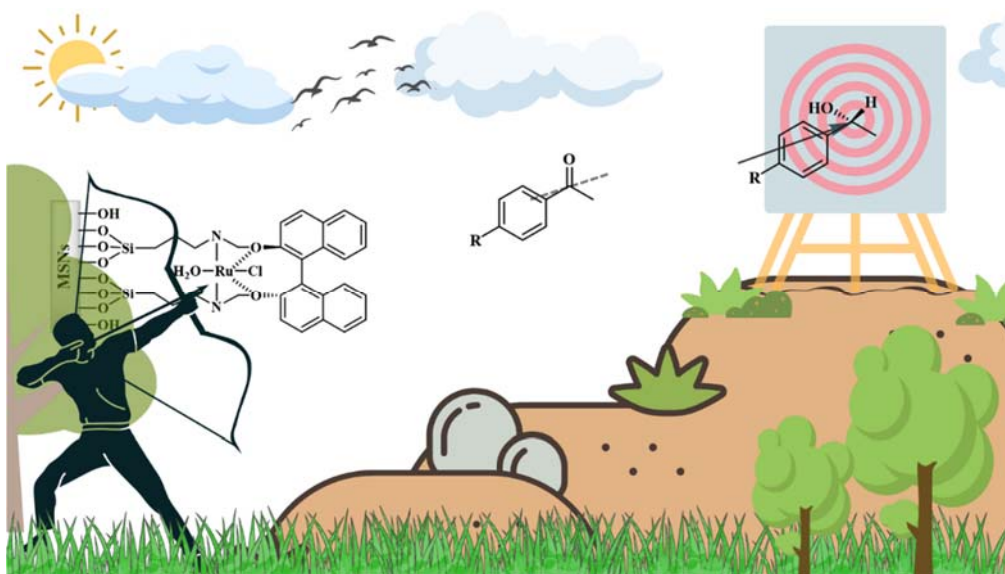# Asymmetric hydrogenation using a covalently immobilized Ru-BINOL-AP@MSNs catalyst

3.1 Introduction:

Asymmetric reduction of unsaturated compounds presents an excellent opportunity for introducing stereogenic elements along with new functionalities into the structure of organic compounds. As a result, this process has become one of the most popular methods of asymmetric synthesis, and it has been used to prepare a diverse of organic scaffolds of biological interest. It is notable that, among the methodologies currently available for this purpose, hydrogen-transfer reduction occupies the second prominent position, followed by asymmetric hydrogenation using molecular hydrogen.[1,2] Aside from excellent selectivities and yields, most of the literature-reported methods require a stoichiometric amounts of vulnerable chemicals or the utilization of insecure hydrogen gas at elevated pressure.[3] Despite the availability of hydrogen donors (2-propanol), as well as the fact that it is cost effective, convenient, and need not rely on complicated experimental setups such as browbeat reactors, the hydrogen-transfer reduction reaction is gaining popularity.[4] On the other hand, homogeneous metal catalysts (Ru and Ir complexes) are frequently used for these chemical reactions.[5,6] Nonetheless, a homogeneous catalyst can generally be recovered and its products purified using methods such as purification, extraction or centrifugation, but complete removal is difficult to achieve even with these methods.[7] Aside from recycling catalysts, catalyst should also be removed from the reaction mixture at a level of parts per million. The reason these workups are less suitable for industrial applications is that they are time-consuming, tedious, as well as energy-consuming.

The chiral binaphthyl plays an important role as an auxiliary chiral component.[8] There are various enantioselective catalytic systems based on BINOLs and BINAPs developed by Noyori et al.[9] The BINOL-based scaffold has been immobilized by grafting it to organic and inorganic supports. However, we have been researching the immobilization of chiral BINOL species using contemporary approach. Furthermore, ruthenium metal hydrides produced by asymmetric transfer hydrogen (ATH) are highly susceptible to air, making their isolation and reusability extremely challenging. There have been a number of heterogeneous variants developed to circumvent these problems, including polymers,[10,11] carbon-nanotube,[12] ionic liquids,[13–15] dendrimers,[16–18] inorganic materials (like Fe_3O_4 nanoparticles),[19,20] or organic/inorganic materials.[7,12] Most of these systems require high temperatures, extended reaction times, an uplifted catalyst loading, excess base, and

a time-consuming recovery process, like filtration or centrifugation. The employment of both chiral auxiliaries and transition metal catalysts is often rather expensive, which is why silica supports have been used to immobilize enantioselective catalyst systems to ensure that catalyst separation and recycling is facilitated.[21–23] The use of binaphthyls chirality in silica supports has been studied and used in asymmetric catalysis in particular.[24,25] Mesoporous amorphous silica nanoparticles (MSNs) have proven valuable as supported materials because they can be obtained in large quantities, possess a large surface-to-volume ratio, are stable at high temperatures and pH, and can be functionalized in a number of different ways.[26–30] In light of the rising appreciation for MSNs as promising platforms, the proposed work aimed to develop a state-of-the-art method to synthesize exceedingly competent and enantioselective system by grafting Ru(III) (*S*) BINOL moiety onto MSNs. It demonstrated unique activity in stereoselective transfer hydrogenation, with 84.38% conversion and enantioselectivity > 90% for the *R*-isomer. Adding to the excitement, the newly synthesized catalyst retains its activity even after undergoing recycling for five consecutive cycles.
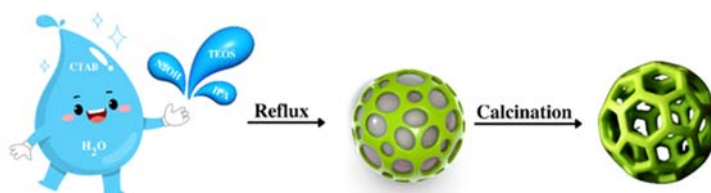
Scheme 3.1 Synthesis of Mesoporous Silica Nanoparticles MSNs.
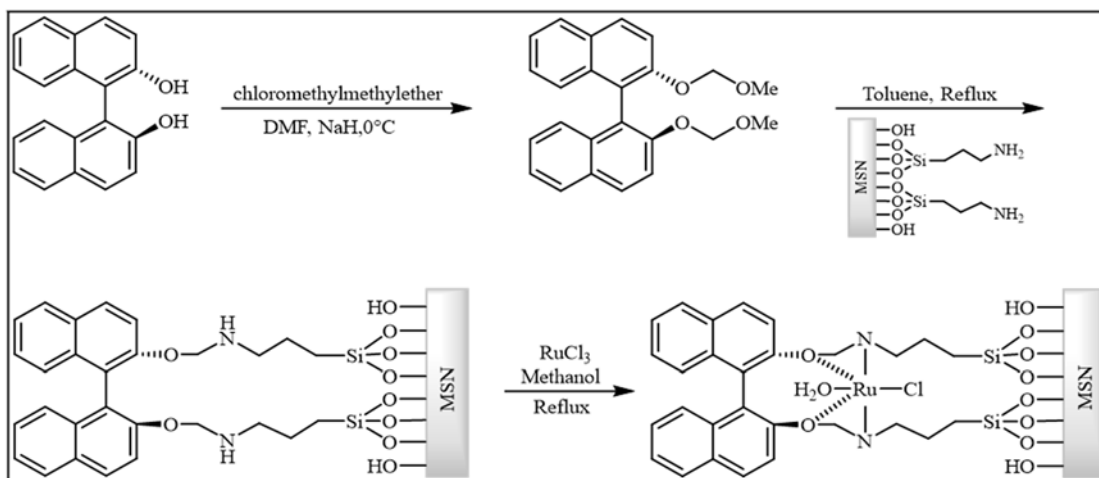
Scheme 3.2 A state-of-the-art pathway for synthesizing Ru-BINOL-AP@MSNs.

3.2 Experimental Section

3.2.1 Synthesis of mesoporous silica nanoparticles (MSNs)

A previously published method [31] was modified to some extent to synthesize the MCM-41 type of MSNs. 480 ml of distilled water and 3.5 ml of 2 M NaOH solution were intimately mixed together, Subsequently the addition of 1 g of surfactant (CTAB) and 5 ml of isopropyl alcohol as a co-surfactant with continuous stirring and then, a homogenous solution was created by gently heating the mixture. Then, a white slurry was produced by adding 5 ml of TEOS very slowly (dropwise) while stirring vigorously. The finished product was filtered after two hours, washed multiple times with CH_3OH and distilled water, dried at 70 °C, and then calcined for six hours at 550 °C (*Scheme 3.1*).

3.2.2 Synthesis of (3-aminopropyl)trimethoxysilane grafted onto MSNs (AP@MSNs)

Using a reported post-synthetic grafting technique[32], an amine-functionalized MSNs was synthesized. Here in this method, 1.0 g of pre-dried calcinated MSNs were mixed with 10 mL dry toluene within a round-bottom flask. In an argon atmosphere, the mixture obtained was subjected to continuous stirring and heated to a reflux temperature for a period of 1 hour. Subsequently, (3-aminopropyl)trimethoxysilane (5.5 mmol, 1 mL) was carefully added drop by drop to the ongoing reaction mixture, while maintaining continuous stirring. The reaction was allowed to progress for a duration of 24 hours. The resulting product was initially subjected to filtration and subsequently washed multiple times in succession with toluene and acetone. The solid mass that ensued was then dried in a vacuum oven at 110°C for 6 hours, resulting in the formation of amine-functionalized MSNs.

3.2.3 Preparation of 2-(methoxymethoxy)-1-(2-(methoxymethoxy)-naphthalen-1-yl)naphthalene (MMNN)

The title compound was synthesized as per the reported method using *S*-BINOL as the starting material.[33] In the first step, 40% suspension of sodium hydride in mineral oil (1.76 g, 29.5

mmol) was dispersed in dimethylformamide (DMF) (20 ml) and then mixed in a solution of *S*-BINOL (1.20 g, 4.2 mmol) at 0°C. After 1 h of stirring at 0°C, the mixture was then given 1.25 ml of methoxy methyl chloride (16.65 mmol), and stirred for an further 1 hour at 0°C. The reaction mixer was maintained for 3 hours at room temperature. This mixture was then cooled with distilled water and extracted with diethyl ether (60 ml), followed by saturated $NaHCO_3$ and 10% brine solutions were used to wash the extracted organic layer to get the final product. The compound was allowed to recrystallize with diethyl ether as a solvent at room temperature.

3.2.4 Synthesis of MMNN grafted onto amine-functionalized MSNs

A suspension containing 1.0 g of amine-functionalized MSNs was prepared in 10 mL of toluene. This suspension was heated with continuous stirring under an argon atmosphere at its reflux temperature for 1 hour. Subsequently, while maintaining the same conditions, MMNN (1.0 mmol, 0.37 g) was introduced into the reaction mixture and left to react for 24 hours. Following the reaction, the product was filtered, subjected to multiple washes with acetone and toluene, and ultimately dried in an air oven at 120 °C for a period of 6 hours to obtain the final product.

3.2.5 Synthesis of chiral Ru-BINOL-AP@MSNs

S-BINOL-amine-functionalized MSNs (1.0 g) were dispersed in methanol (10 mL) and heated for 15 minutes with incessant stirring under an inert atmosphere. The reaction mixture was then treated with $RuCl_3 \cdot 3H_2O$ (1.0 mmol, 0.26 g) at a reflux temperature. After the reaction prolonged for 6 hours, the solid catalyst was then filtered, washed multiple times with methanol and finally dried at 120°C in a heating oven for 6 hours (*Scheme 3.2*).

3.2.6 Catalytic Activity

An asymmetric hydrogenation reaction is performed in which the ketone is converted into an alcohol in an asymmetric manner, which was used to determine the catalytic capacity of Ru-BINOL-AP@MSNs. A catalyst (0.05 g), acetophenone (120.15 mg, 1 mmol), KOH (112.20 mg, 2 mmol) and isopropyl alcohol (10 ml) were added to a 50 mL three angled neck round-bottom

flask (RBF) and stirred continuously for 12 h at 80°C in an argon atmosphere. It was then filtered to remove the solid catalyst and collected the filtrate. The chiral-phase HPLC was used to determine the conversion using Chiralpak OJ-H column; n-hexane/ isopropanol (95/05) system.[34–37] Under the optimized conditions, we also catalytically tested other acetophenone derivatives such as 4-Br acetophenone, 4-Cl acetophenone, 4-MeO acetophenone, 4-OH acetophenone, and 4-NH$_2$ acetophenone under the optimized conditions.

3.3 Results and Discussion

3.3.1 X-ray Diffraction Patterns
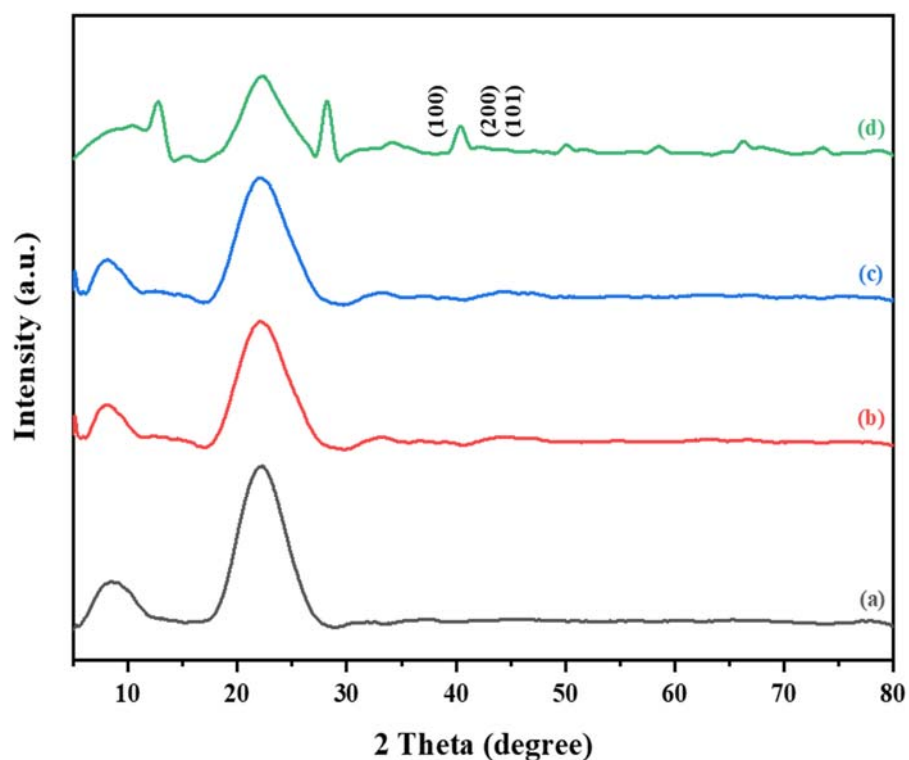
Figure 3.1 XRD patterns (a) MSNs, (b) AP@MSNs, (c) BINOL-AP@MSNs and (d) Ru-BINOL-AP@MSNs.

The XRD measurements were performed in order to ensure that the material obtained has an ordered structure as well as the presence of ruthenium metal ions. *Figure 3.1* presents the diffractograms recorded for MSNs, AP@MSNs, BINOL-AP@MSNs, and Ru-BINOL-AP@MSNs compounds. There were three peaks exhibited in the XRD pattern of MSNs at $2\theta =$ 38.4°, 42.2°, and 44.1° corresponding to the planes (1 0 0), (2 0 0), and (1 0 1), respectively. The XRD pattern of Ru-BINOL-AP@MSNs confirmed the presence of Ru as low intensity peak at 2θ = 40.3°. This indicates the mesoporous materials have a high crystallinity and hexagonally ordered pores. Functionalization, and thus a subside in the uniformity of the hexagonal mesostructure, may be the cause of the disappearance of XRD peaks in subsequent compounds. In comparison to MSNs, the XRD pattern for Ru metal in silica has a lower intensity, which indicates that the catalyst preparation process involved a lower loading of the metal ion precursor. When the XRD data of neat MSNs, AP@MSNs, and BINOL-AP@MSNs with Ru doped Ru-BINOL-AP@MSNs catalyst were compared, all samples displayed a characteristic wide peak spanning from 15° to 30°, indicative of amorphous silica, a finding that aligns well with the results from HRTEM analysis.[38–40]

3.3.2 Scanning electron microscopy
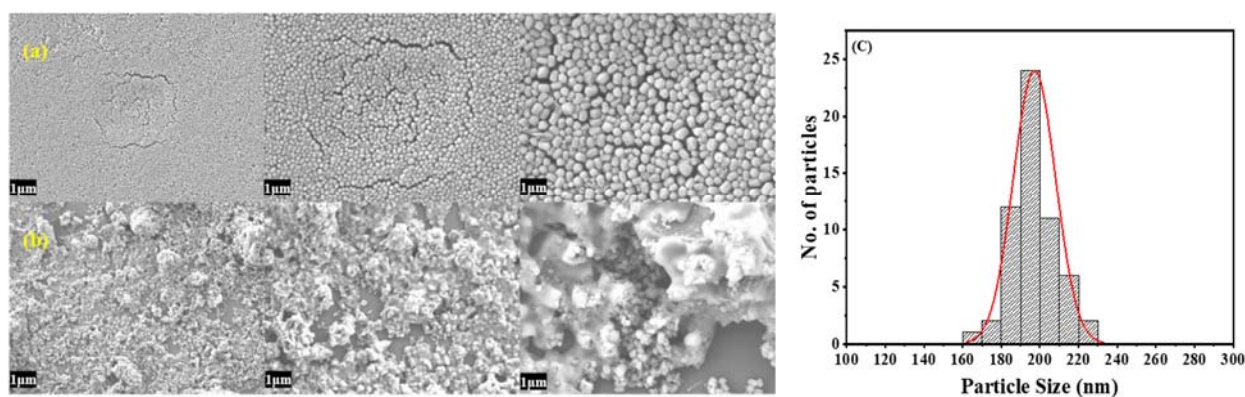
Figure 3.2 FESEM images of (a) MSNs (b) Ru-BINOL-AP@MSNs and (c) Histogram graph of MSNs.

Figures 3.2 (a) and (b) depict FESEM images of as-synthesized MSNs and Ru-BINOL-AP@MSNs, respectively. The SEM images of MSNs and Ru-BINOL-AP@MSNs were compared

to the initial support to ascertain the size and shape of the catalyst. A mono-dispersed spherical particle morphology was observed in the first sample, with particle sizes between 160 and 230 nm. Using ImageJ software, the average size of MSNs was determined to be 200±5 nm, as depicted in *Figures 3.2* (c). The spherical morphology of the MSNs has been preserved, in accordance with the XRD analysis, as shown in *Figures 3.2* (a) and (b), which show both samples have a spherical morphology with a mean diameter below 230 nm. This indicates functionalization did not significantly alter the shape and size of nanoparticles.[41,42]

### 3.3.3 Transmission electron microscopy
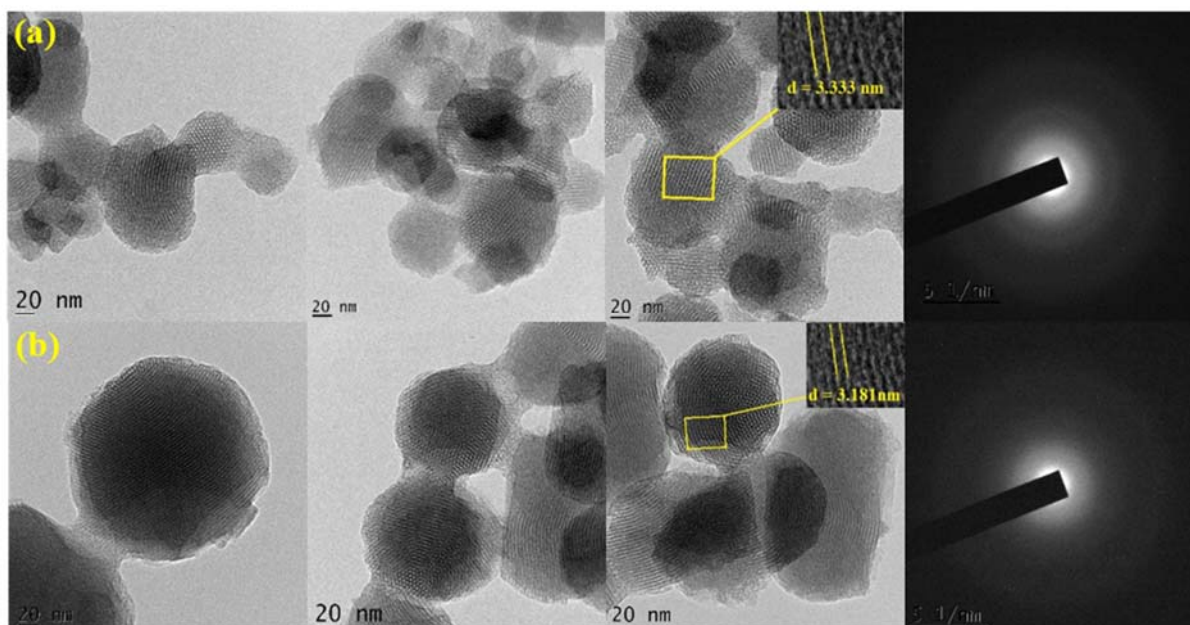
Figure 3.3 HRTEM pictures of (a) MSNs (b) Ru-BINOL-AP@MSNs.

The mesoporous structure of MSNs was characterized using transmission electron microscopy (TEM). Typical micrographs of the as-synthesized compounds are shown in *Figures 3.3.* As shown in *Figure 3.3* (a), mesoporous silica exhibited an array of highly ordered hexagonal pores with typical MSNs properties. The macroscopic hexagonal features of these materials are very consistent with their mesoscopic hexagonal structural units, suggesting that they were formed

by stacking silicate micelles rather than through sol-gel phase transformation. As shown *Figure 3.3* (b), the organic scaffold was incorporated into the MSNs matrix *in situ* without altering the hexagonal pore orders. Selected Area Electron Diffraction (SAED) was employed for both MSNs and Ru-BINOL-AP@MSNs to assess their crystallinity. The SAED analysis on the ensemble of individual particles revealed diffused spots characteristic of amorphous materials, providing further confirmation of the amorphous nature of the silica. Through TEM, the morphologies and microstructures of the obtained MSNs samples can be clearly revealed, where nanosized particles can be reliably observed as elongated or near spheres.[43]

3.3.4 X-ray Photo electronic spectroscopy
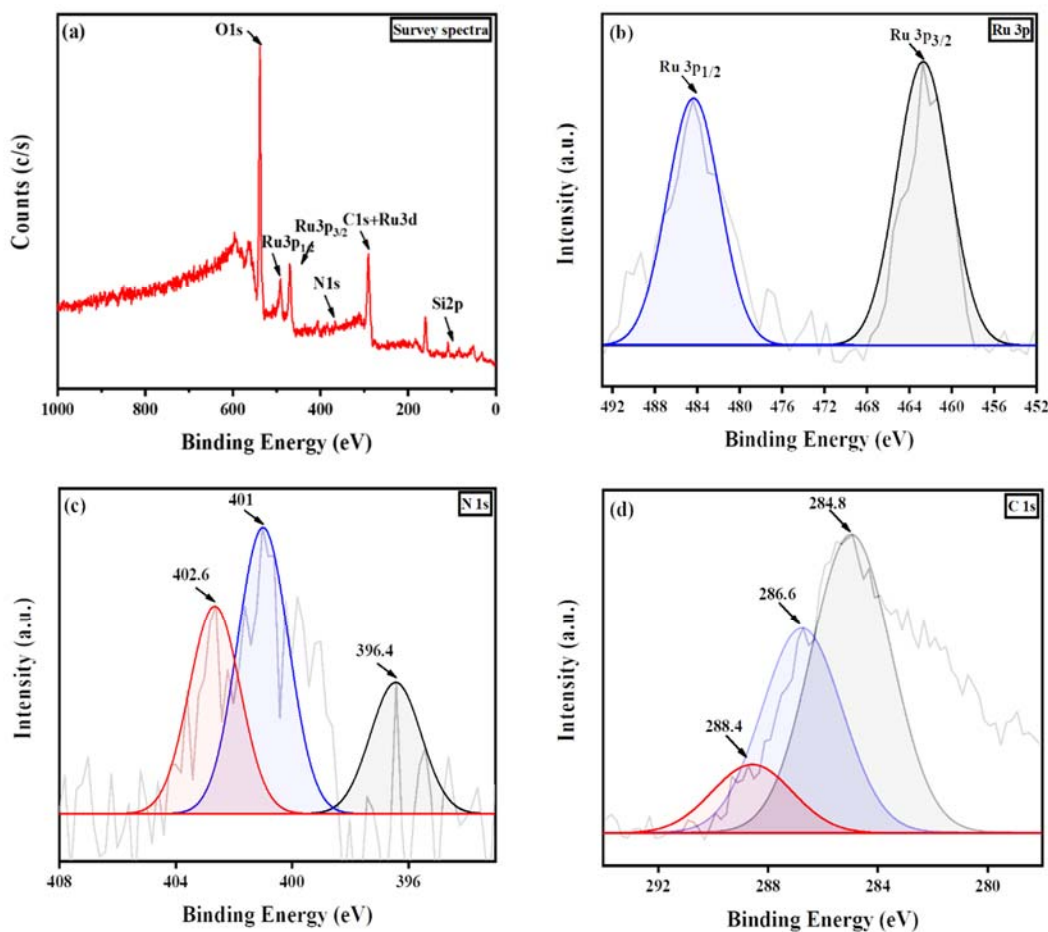
Figure 3.4 XPS spectra of Ru-BINOL-AP@MSNs: (a) survey spectra (b) Ru 3p, (c) N 1s and (d) C 1s.

The X-ray photoelectron spectroscopy (XPS) was used to both determine the Ruthenium oxidation state and to confirm the organic moiety immobilization onto the MSNs matrix. An XPS analysis of Ru-BINOL-AP@MSNs containing survey spectra is shown in *Figure 3.4* (a), illustrating the presence of C, N, O, and Ru elements onto the surface of the catalyst. The binding energy of Ru $3d_{5/2}$ overlayed with that of C 1s, requiring the deconvolution of the XPS Ru $3p_{3/2}$ profile to distinguish Ru species. According to *Figure 3.4* (b), the binding energies of Ru 3p for Ru-BINOL-AP@MSNs are 462.7 and 484.3 eV for $3p_{3/2}$ and $3p_{1/2}$ of Ru, respectively. This indicates that Ru(+3) ions have been reduced completely to Ru(0). Contrarily, the N 1s spectrum (*Figure 3.4* (c)) is deconvoluted into three peaks that are observed at energies that accord with the C-N-C, N-(C)$_3$, and C-N-H bonds, respectively, at 398.5 eV, 400.0 eV, and 401.2 eV. Besides, the existence of chemically diverse carbons in the high-resolution C 1s XPS spectrum (*Figure 3.4* (d)) validates the grafting of BINOL onto MSNs.[44–47] Moreover, ICP-AES analysis data exhibits a weight percentage of Ru of 10.10%, which is consistent with XPS measurements.[48]

3.3.5 FTIR spectra
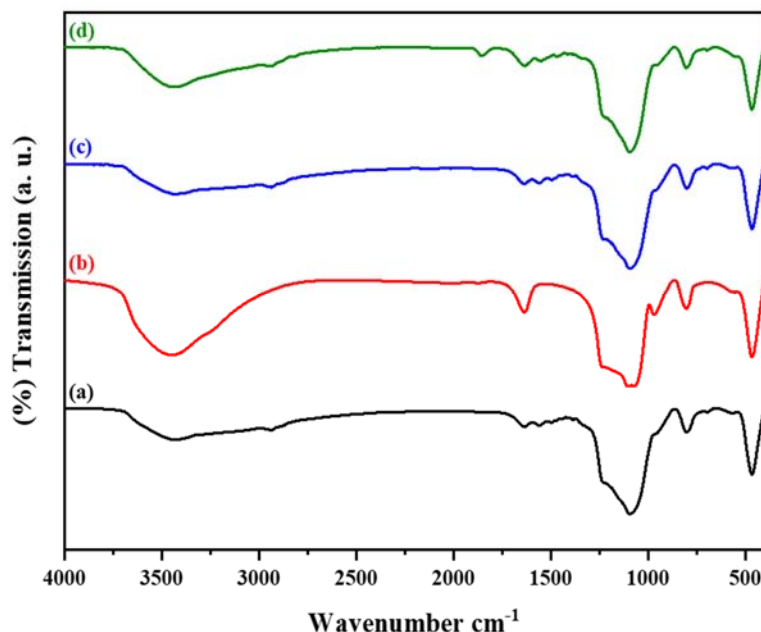
Figure 3.5 FTIR spectra of (a) MSNs, (b) AP@MSNs, (c) BINOL-AP@MSNs and (d) Ru-BINOL-AP@MSNs.

FTIR spectra of MSNs, AP@MSNs, BINOL-AP@MSNs and, Ru-BINOL-AP@MSNs are presented in *Figure 3.5*. The FTIR spectra of heterogenized systems, namely AP@MSNs, BINOL-AP@MSNs and, Ru-BINOL-AP@MSNs, are consistent with the predicted chemical structure of the organic scaffolds (*Figure 3.5*). In addition, in contrast to the spectra of MSNs, a couple of new peaks in the FTIR spectra of heterogenized systems were seen at ~2935 (C-H stretching vibrations), ~1630 (C-N vibration), and ~1470 (C-C stretching vibration) cm^{-1}, indicating the establishment of the hybrid organic-inorganic systems. Additionally, silanol capping with a trimethylsilyl group (TMS) on siliceous supports resulted in a substantial reduction in the free Si-OH stretching band observed at around 3400 cm^{-1} in the FTIR spectra of AP@MSNs, BINOL-AP@MSNs, and Ru-BINOL-AP@MSNs (*Figure 3.5* (b-d)). A reduction in relative intensity of peaks at 3475 cm^{-1} and 3382 cm^{-1} was observed after BINOL and anchoring of Ru metal ions onto MSNs, and the characteristic band (due to -NH bending vibration) observed at 1634 cm^{-1} was found to disappear, indicating the formation of a C–N bond after BINOL and anchoring of Ru metal ions.[49–51]

3.3.6 ^{13}C CP MAS NMR spectra
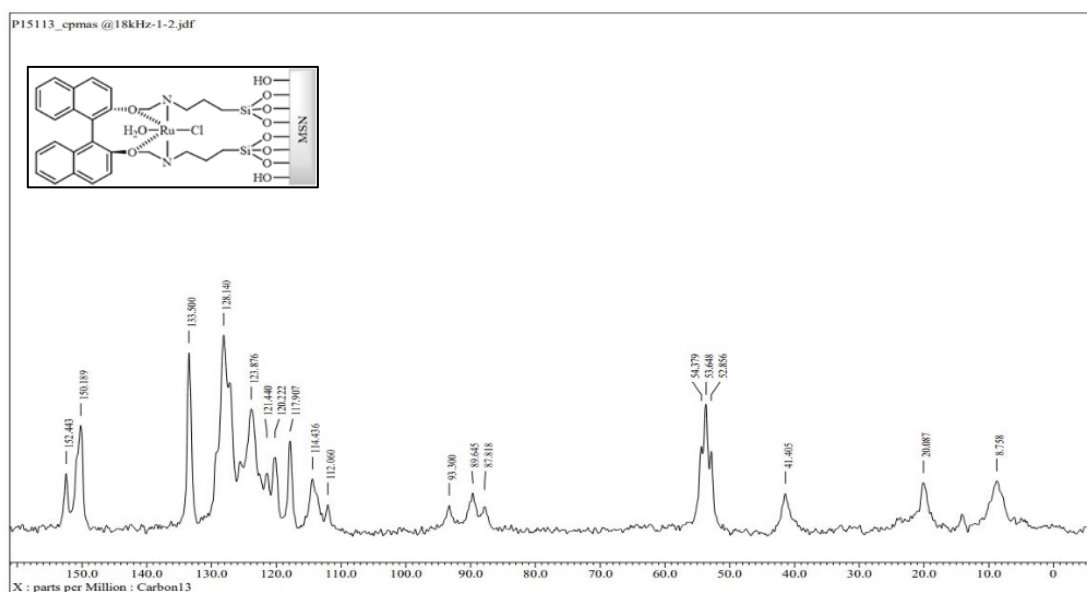
Figure 3.6 ^{13}C CP MAS NMR spectrum of Ru-BINOL-AP@MSNs.

^{13}C CP MAS spectrum of Ru-BINOL-AP@MSNs, shown in *Figure 3.6*, exhibits peaks at 63, 41, 28, and 9 ppm due to MAPTES surface modification, 120-155 ppm for aromatic carbons from (*S*)-BINOL's naphthyl groups, and 170 ppm (CH$_2$-NH group), which shows that BINOL was successfully attached to silica.[50]

3.3.7 BET analysis
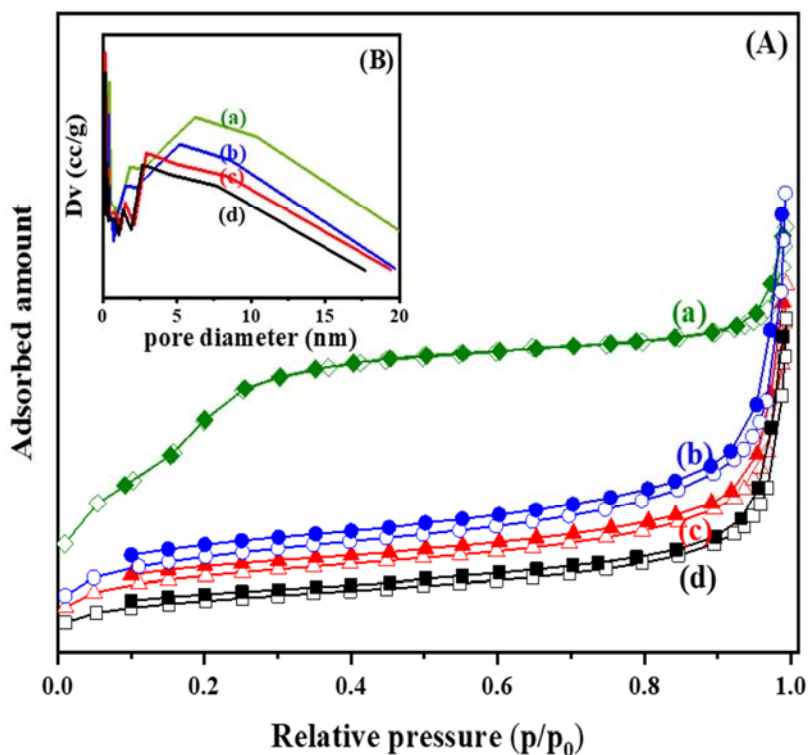
Figure 3.7 (A) N$_2$ adsorption− desorption isotherms of (a) MSNs, (b) AP@MSNs, (c) BINOL-AP@MSNs and (d) Ru-BINOL-AP@MSNs; (B) BJH pore size distributions of (a) MSNs, (b) AP@MSNs, (c) BINOL-AP@MSNs and (d) Ru-BINOL-AP@MSNs.

Table 3.1 Textural parameters of catalysts and catalyst precursors

| Sample	Surface area/m^2 g^{-1}	Pore volume/cm^3 g^{-1}	Average pore diameter/nm
MSNs	1048.32	0.91	6.2
AP@MSNs	106.31	0.82	5.2
BINOL-AP@MSNs	101.3	0.58	2.9
Ru-BINOL-AP@MSNs	89.02	0.38	2.6

Figure 3.7(A) shows N_2 adsorption-desorption isotherms and pore size distribution curves of MSNs, AP@MSNs, BINOL-AP@MSNs, and Ru-BINOL-AP@MSNs. A revocable type IV adsorption-desorption isotherm was observed in the neat siliceous MSNs, which is typical of mesoporous materials. The neat siliceous MSNs had a specific BET surface area of 1048 m^2 g^{-1} (*Table 3.1*). The isotherms of functionalized MSNs, such as AP@MSNs, BINOL-AP@MSNs, and Ru-BINOL-AP@MSNs, on the other hand, displayed a lower N_2 uptake, indicating a reduction in specific surface area and pore volume (*Table 3.1*). Furthermore, the p/p_0 coordinate of the inflection point and the capillary condensation step height both decreased, indicating organic species grafting at the internal silica surface altered the pore size distributions in these materials (*Figure 3.7*(B)).[32]

3.3.8 Thermogravimetric study
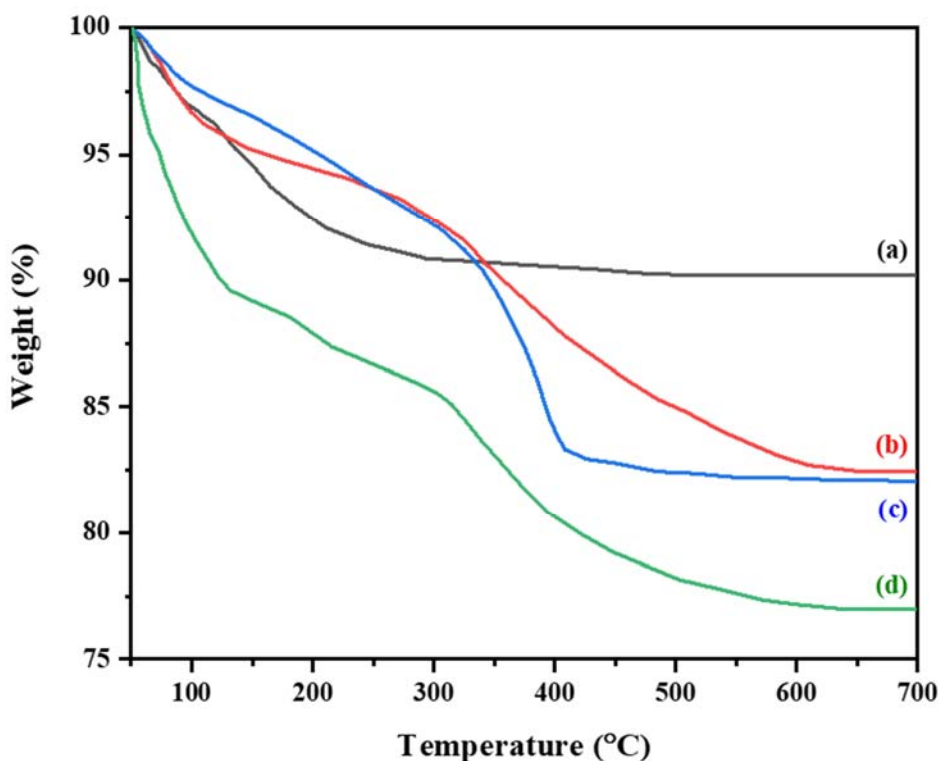
Figure 3.8 TGA curves of (a) MSNs, (b) AP@MSNs, (c) BINOL-AP@MSNs and, (d) Ru-BINOL-AP@MSNs.

The TGA curves of neat MSNs, AP@MSNs, BINOL-AP@MSNs, and Ru-BINOL-AP@MSNs are shown in *Figure 3.8*. According to *Figure 3.8*, neat MSNs showed only one step of degradation (up to 300 °C) with an observed mass loss of 9.82%, which might be due to desorption of the physiosorbed water and dehydroxylation of the surface silanol groups present on MSNs. AP@MSNs and BINOL-AP@MSNs, on the other hand, demonstrated two consecutive weight losses, one at temperatures below 300 °C and the other at above 300 °C. The decomposition of aminopropyl silane groups resulted in an additional 10.27% weight loss (above 300°C) in AP@MSNs as compared to MSNs after accounting for the weight loss that is associated with the

dehydroxylation of some residual silanol groups (below 300°C). Furthermore, BINOL-AP@MSNs showed 10.1% weight loss, which might be due to BINOL-AP organic scaffolds. Decomposition of the Ru-BINOL-AP@MSNs occurs in three distinct steps. Lattice water molecules are lost in the first step, which occurs in the temperature range of 50 to 140 °C, where a mass loss of 10.38% was observed. A second stage occurs between 140 and 300 °C with a mass loss of 4.06% observed. This is most likely due to the decomposition of one water molecule and one chloride ion coordinated to ruthenium metal ion. With heating; the decomposition of the aminopropyl and BINOL based organic scaffolds was followed. It was assumed that the third stage, which takes place in the temperature range 300–600°C, corresponds to the breakdown of the aminopropyl and BINOL-based organic scaffolds. After calculating the weight loss (obs. 8.95%) resulting from organic scaffold degradation above 300°C. [52–54]

3.4 Catalytic activity

In this work, we looked into the potential of Ru-BINOL-AP@MSNs an archetypal catalyst for asymmetric hydrogenation reaction (*Scheme 3.3*). 10 mL of 2-propanol acting as both a solvent and a source of hydrogen was mixed with 1 mmol substrate and 0.05g of catalyst (Ru-BINOL-AP@MSNs) in a 50 mL reaction vessel. Employing acetophenone as a representative substrate, optimal reaction conditions for transfer hydrogenation reaction were determined. It was evident that 80°C temperature was imperative for improving yield with KOH as the base, however, a reduction in yield was observed with less than 2 mmol of the base injected. In addition, Ru-BINOL-AP@MSNs without base, as well as without either catalyst or base, or both, failed to yield any product. Acetophenone in isopropyl alcohol (IPA) underwent asymmetric transfer hydrogenation in just 12 hours, producing 84.38% of 1-phenyl ethanol with a 90.80% ee.
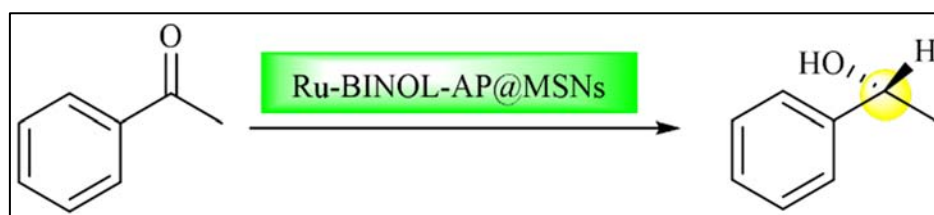
Scheme 3.3 Asymmetric transfer hydrogenation reaction catalyzed by Ru-BINOL-AP@MSNs

3.4.1 Acetophenone derivatives

Moreover, other acetophenone derivatives have also been tested over Ru-BINOL-AP@MSNs catalyst under optimized conditions as shown in *Table 3.2*. Both electron-withdrawing groups (4-bromoacetophenone and 4-chloroacetophenone) and electron-donating groups (4-methoxyacetophenone, 4-hydroxyacetophenone, and 4-aminoacetophenone) can be successfully hydrogenated to produce high yields and enantioselectivities for the corresponding alcohols.

Table 3.2 Different types of acetophenone derivatives, the % conversion and excess of enantiomer (ee) catalyzed by Ru-BINOL-AP@MSNs in the asymmetric hydrogenation reaction

Entry	Substrates(R)	Conversion(%) [a]	ee (%) [b]
1	4-Br acetophenone	84	92
2	4-Cl acetophenone	83	87
3	4-OMe acetophenone	80	86
4	4-OH acetophenone	76	83
4	4-NH$_2$ acetophenone	74	81

[a] Conversion Determined by normal HPLC analysis. [b] ee Determined by chiral-phase HPLC analysis (Chiralpak OJ-H)

3.4.2 Recyclability test

For asymmetric transfer hydrogenation, we have performed a recyclability test on the Ru-BINOL-AP@MSNs catalyst to demonstrate its heterogeneous nature and their results are shown in *Table 3.3* and depicted in *Figure 3.9*. The catalyst Ru-BINOL-AP@MSNs can be quantitatively recovered by filtration during a catalytic recyclability test, but the product can be isolated from the reaction mixture by extraction with diethyl ether, producing a clean product without the need for additional purification. Additionally, Ru-BINOL-AP@MSNs catalyst recyclability was examined

in 5 runs, yields gradually declining after the third run despite consistently high enantioselectivities (*Table 3.3*).

Table 3.3 Recyclability test of the asymmetric hydrogenation reaction catalyzed by Ru-BINOL-AP@MSNs.

Consecutive runs (Reuse)	Conversion (%)[a]	Excess enantiomer (ee) (%)[b]
0	84	91
1	83	86
2	80	85
3	75	84
4	72	82

[a] Conversion Determined by normal HPLC analysis. [b] ee Determined by chiral-phase HPLC analysis (Chiralpak OJ-H)

Reaction condition: Acetophenone (1 mmol), IPA (10 mL), Ru-BINOL-AP@MSNs (0.05 g), 80 °C, 12 h.
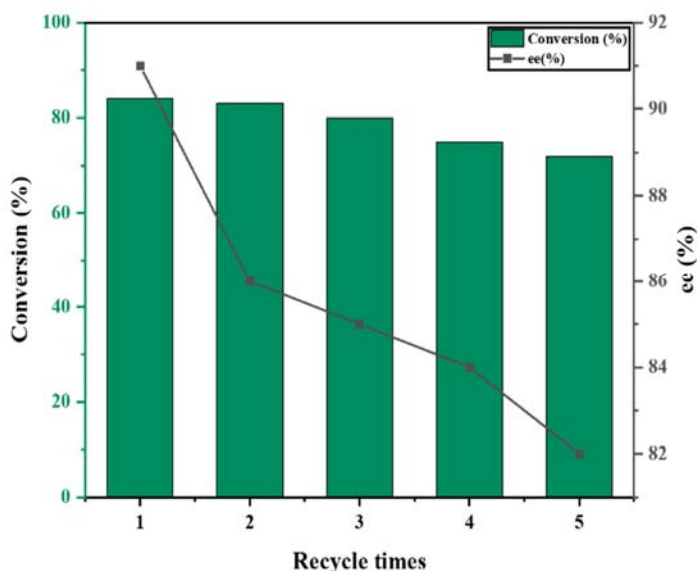
Figure 3.9 Recyclability test of Ru-BINOL-AP@MSNs catalyst over asymmetric hydrogenation reaction

3.5 Conclusions

This study presents a state-of-the-art pathway for the design of chiral Ru-BINOL functionalized mesoporous silica nanoparticles, Ru-BINOL-AP@MSNs, without the need for any protecting or deprotecting steps, which were competently corroborated through various analytical techniques. This hybrid catalyst, which was demonstrated to be stable and efficient, was used for asymmetric hydrogenation in isopropyl alcohol (IPA). Additionally, Ru-BINOL-AP@MSNs catalyst could be recycled and reused at least five more times without significantly losing its effectiveness. The Ru-BINOL-AP@MSNs catalyst has been found to have the following advantages: high yields of product, low catalyst requirement, easy workup, simple methodology, and reusability without significant loss of activity. By employing this potent technique, we aim to develop more sturdy, multifaceted, stereoselective, and recyclable chiral BINOL-based organocatalysts for asymmetric organic transformations.

3.6 References

1.   Gladiali, S. & Alberico, E. Asymmetric transfer hydrogenation: Chiral ligands and applications. *Chem. Soc. Rev.* **2006,** 35, 226–236.

2.   Din Reshi, N. U., Senthurpandi, D. & Samuelson, A. G. A mechanistic study of transfer hydrogenation catalyzed by cyclometallated ruthenium half-sandwich complexes. *J. Organomet. Chem.* **2018,** 866, 189–199.

3.   Sudhakar, M. *et al.* Hydroxyapatite as a novel support for Ru in the hydrogenation of levulinic acid to γ-valerolactone. *Catal. Commun.* **2014**, 50, 101–104.

4.   Saluzzo, C. & Lemaire, M. Homogeneous-Supported Catalysts for Enantioselective Hydrogenation and Hydrogen Transfer Reduction. *Adv. Synth. Catal.* **2002**, 344, 915–928.

5.   McDonald, A. R., Müller, C., Vogt, D., van Klink, G. P. M. & van Koten, G. BINAP-Ru and -Rh catalysts covalently immobilised on silica and their repeated application in asymmetric hydrogenation. *Green Chem.* **2008,** 10, 424–432.

6.   Yu, J. *et al.* Discovery and development of ferrocene-based tetradentate ligands for Ir-catalysed asymmetric hydrogenation of ketone. *Green Synth. Catal.* **2022,** 3, 175–178.

7.   Eichenseer, C. M., Kastl, B., Pericàs, M. A., Hanson, P. R. & Reiser, O. Synthesis and Application of Magnetic Noyori-Type Ruthenium Catalysts for Asymmetric Transfer Hydrogenation Reactions in Water. *ACS Sustain. Chem. Eng.* **2016,** 4, 2698–2705.

8.   Yang, G., Guo, D., Meng, D. & Wang, J. NHC-catalyzed atropoenantioselective synthesis of axially chiral biaryl amino alcohols via a cooperative strategy. *Nat. Commun.* **2019**, 10, 1–6.

9.   Noyori, R. & Ohkuma, T. Asymmetric catalysis by architectural and functional molecular engineering: Practical chemo- and stereoselective hydrogenation of ketones. *Angew. Chemie - Int. Ed.* **2001**, 40, 40–73.

10.   Altava, B., Burguete, M. I., García-Verdugo, E. & Luis, S. V. Chiral catalysts immobilized on achiral polymers: Effect of the polymer support on the performance of the catalyst. *Chem. Soc. Rev.* **2018**, 47, 2722–2771.

11. Marcos, R., Jimeno, C. & Pericàs, M. A. Polystyrene-supported enantiopure 1,2-diamines: Development of a most practical catalyst for the asymmetric transfer hydrogenation of ketones. *Adv. Synth. Catal.* **2011**, 353, 1345–1352.

12. Uruş, S., Adıgüzel, H., Keleş, M. & Karteri, İ. Multi-walled carbon nanotube supported aminomethylphosphine-Ru(II) complexes: Optical behavior and catalytic properties in transfer hydrogenation of acetophenone derivatives. *Fullerenes Nanotub. Carbon Nanostructures* **2017**, 25, 133–141.

13. Hejazifar, M., Pálvölgyi, Á. M., Bitai, J., Lanaridi, O. & Bica-Schröder, K. Asymmetric Transfer Hydrogenation in Thermomorphic Microemulsions Based on Ionic Liquids. *Org. Process Res. Dev.* **2019**, 23, 1841–1851.

14. Li, X., Sun, Y., Wang, S. & Jia, X. Stable Chiral Ruthenium Complex Catalyst Based on Polymer Ionic Liquid for Asymmetric Transfer Hydrogenation of Aliphatic Ketones in Water. *ACS Appl. Polym. Mater.* **2020**, 2, 1268–1275.

15. Modi, C. K., Panwala, S., Vithalani, R. & Patel, D. Ionic liquid infiltrated within metal loaded zeolites for Baeyer–Villiger oxidation reaction under solvent-free condition. *J. Porous Mater.* **2018** ,25, 871–883.

16. Chen, Y. C. *et al.* Synthesis of dendritic catalysts and application in asymmetric transfer hydrogenation. *J. Org. Chem.* **2005**, 70, 1006–1010.

17. Cotman, A. E., Lozinšek, M., Wang, B., Stephan, M. & Mohar, B. Trans-Diastereoselective Ru(II)-Catalyzed Asymmetric Transfer Hydrogenation of α-Acetamido Benzocyclic Ketones via Dynamic Kinetic Resolution. *Org. Lett.* **2019**, 21, 3644–3648.

18. Chandra, S., Patel, M. D., Lang, H. & Bahadur, D. Dendrimer-functionalized magnetic nanoparticles: A new electrode material for electrochemical energy storage devices. *J. Power Sources,* **2015**, 280, 217–226.

19. Hudson, R., Chazelle, V., Bateman, M., Roy, R., Li, C.-J., & Moores, A. Sustainable Synthesis of Magnetic Ruthenium-Coated Iron Nanoparticles and Application in the Catalytic Transfer Hydrogenation of Ketones. *ACS Sustain. Chem. Eng.* **2015**, 3, 814–820.

20. Nasir Baig, R. B. & Varma, R. S. Magnetic silica-supported ruthenium nanoparticles: An

efficient catalyst for transfer hydrogenation of carbonyl compounds. *ACS Sustain. Chem. Eng.* **2013**, 1, 805–809.

21. Faisal, S., Maity, P. K., Zang, Q., Samarakoon, T. B., Sourk, R. L., & Hanson, P. R. Application of Silica-Supported Alkylating Reagents in a One-Pot, Sequential Protocol to Diverse Benzoxathiazepine 1,1-Dioxides. *ACS Comb. Sci.* **2016**, 18, 387–393.

22. Ley, S. V., Baxendale, I. R., Bream, R. N., Jackson, P. S., Leach, A. G., Longbottom, D. A., Nesi, M., Scott, J. S., Storer, R. I., & Taylor, S. J. Multi-step organic synthesis using solid-supported reagents and scavengers: A new paradigm in chemical library generation. *J. Chem. Soc. Perkin Trans.* **2000**, 1, 3815–4195.

23. Kureshy, R. I. Sulfonic acid functionalized mesoporous SBA-15 as an efficient and recyclable catalyst for the synthesis of chromenes from chromanols. *Catal. Commun.* **2009**, 10, 572–575.

24. Valverde-González, A. Porous aromatic frameworks containing binaphthyl-dihydroazepine units (cBAPAFs) as catalytic supports for asymmetric reactions. *J. Catal.* **2022**, 413, 434–442.

25. Gross, E., Liu, J. H., Alayoglu, S., Marcus, M. A., Fakra, S. C., Toste, F. D., & Somorjai, G. A. Asymmetric catalysis at the mesoscale: Gold nanoclusters embedded in chiral self-assembled monolayer as heterogeneous catalyst for asymmetric reactions. *J. Am. Chem. Soc.* **2013**, 135, 3881–3886.

26. Lee, J. Y., Kim, M. K., Nguyen, T. L. & Kim, J. Hollow Mesoporous Silica Nanoparticles with Extra-Large Mesopores for Enhanced Cancer Vaccine. *ACS Appl. Mater. Interfaces* **2020**, 12, 34658–34666.

27. Tang, F., Li, L. & Chen, D. Mesoporous silica nanoparticles: Synthesis, biocompatibility and drug delivery. *Adv. Mater.* **2012**, 24, 1504–1534.

28. Estevão, B. M., Miletto, I., Hioka, N., Marchese, L. & Gianotti, E. Mesoporous Silica Nanoparticles Functionalized with Amino Groups for Biomedical Applications. *ChemistryOpen* **2021**, 10, 1251–1259.

29. Sun, H. Mesostructured SBA-16 with excellent hydrothermal, thermal and mechanical

stabilities: Modified synthesis and its catalytic application. *J. Colloid Interface Sci.* **2009**, 333, 317–323.

30.   Shukla, M., Barick, K. C., Salunke, H. G. & Chandra, S. Chiral salen - Ni (II) based spherical porous silica as platform for asymmetric transfer hydrogenation reaction and synthesis of potent drug intermediate montekulast. *Mol. Catal.* **2021**, 502, 111367.

31.   Bhavsar, D., Patel, V. & Sawant, K. Systemic investigation of in vitro and in vivo safety, toxicity and degradation of mesoporous silica nanoparticles synthesized using commercial sodium silicate. *Microporous Mesoporous Mater.* **2019**, 284, 343–352.

32.   Lakhani, P. & Modi, C. K. Spick-and-span protocol for designing of silica-supported enantioselective organocatalyst for the asymmetric aldol reaction. *Mol. Catal.* **2022**, 525, 112359.

33.   Munusamy, S. & Kulathu Iyer, S. A chiral (S)-BINOL based fluorescent sensor for the recognition of Fe(III) and cascade discrimination of α-amino acids. *Tetrahedron Asymmetry,* **2016**, 27, 492–497.

34.   Khamis, N., Clarkson, G. J. & Wills, M. Heterocycle-containing Noyori-Ikariya catalysts for asymmetric transfer hydrogenation of ketones. *Dalt. Trans.* **2022**, 51, 13462-13469.

35.   Dayan, S. *et al.* Synthesis and characterization of SiO2-supported ruthenium complexes containing aromatic sulfonamides: As catalysts for transfer hydrogenation of acetophenone. *J. Chem. Soc. Dalt. Trans.* **2013**, 42, 4957–4969.

36.   Ganesamoorthy, S., Jerome, P., Shanmugasundaram, K. & Karvembu, R. Highly efficient homogeneous and heterogenized ruthenium catalysts for transfer hydrogenation of carbonyl compounds. *RSC Adv.* **2014**, 4, 27955–27962.

37.   Duraczyńska, D., Drelinkiewicz, A., Bielańska, E., Serwicka, E. M. & Lityńska-Dobrzyńska, L. Hydrogenation of acetophenone in the presence of Ru catalysts supported on amine groups functionalized polymer. *Catal. Letters,* **2011**, 141, 83–94.

38.   Szczyglewska, P., Feliczak-Guzik, A. & Nowak, I. A support effect on the hydrodeoxygenation reaction of anisole by ruthenium catalysts. *Microporous Mesoporous Mater.* **2020,** 293, 109771.

39. La-Salvia, N., Lovón-Quintana, J. J., Lovón, A. S. P. & Valença, G. P. Influence of aluminum addition in the framework of MCM-41 mesoporous molecular sieve synthesized by non-hydrothermal method in an alkali-free system. *Mater. Res.* **2017**, 20, 1461–1469.

40. Srivastava, V. Active Heterogeneous Ru Nanocatalysts for CO2 Hydrogenation Reaction. *Catal. Letters,* **2016**, 146, 2630–2640.

41. Jalalzadeh-Esfahani, M., Sedaghat, T., Beheshti, A. & Azadi, R. Immobilization of palladium on benzimidazole functionalized mesoporous silica nanoparticles: catalytic efficacy in Suzuki–Miyaura reaction and nitroarenes reduction. *J. Porous Mater.* **2022**, 29, 1149–1164.

42. Masjedi-Arani, M., Salavati-Niasari, M., Ghanbari, D. & Nabiyouni, G. A sonochemical-assisted synthesis of spherical silica nanostructures by using a new capping agent. *Ceram. Int.* **2014**, 40, 495–499.

43. Pradhan, A. C., Sahoo, M. K., Bellamkonda, S., Parida, K. M. & Rao, G. R. Enhanced photodegradation of dyes and mixed dyes by heterogeneous mesoporous Co-Fe/Al2O3-MCM-41 nanocomposites: Nanoparticles formation, semiconductor behavior and mesoporosity. *RSC Adv.* **2016**, 6, 94263–94277.

44. Fan, L. *et al.* Ru nanoparticles encapsulated in ZIFs-derived porous N-doped hierarchical carbon nanofibers for enhanced hydrogen evolution reaction. *Catal. Sci. Technol.* **2020**, 10, 7302–7308.

45. Harbottle, A. M., Hira, S. M., Josowicz, M. & Janata, J. Lewis Acid Based Sorption of Trace Amounts of RuCl3 by Polyaniline. *Langmuir,* **2016**, 32, 8315–8321.

46. Wang, H., Li, X., Ruan, Q. & Tang, J. Ru and RuO: X decorated carbon nitride for efficient ammonia photosynthesis. *Nanoscale,* **2020**, 12, 12329–12335.

47. Jin, Y., Li, G., Zhang, J., Pu, Y. & Li, W. Effects of potassium additive on the activity of Ru catalyst for acetylene hydrochlorination. *RSC Adv.* **2015**, 5, 37774–37779.

48. Deme, J. Synthesis and catalytic olefin metathesis activity of amberlyst-15 supported cyclic and bicyclic alkyl amino carbene ruthenium complexes. *React. Kinet. Mech. Catal.* **2022**, 135, 2519–2531.

49. Mazzieri, V., Coloma-Pascual, F., Arcoya, A., L'Argentière, P. C. & Fígoli, N. S. XPS, FTIR and TPR characterization of Ru/Al 2 O 3 catalysts. *Appl. Surf. Sci.* **2003**, 210, 222–230.

50. Pathak, K. The synthesis of silica-supported chiral BINOL: Application in Ti-catalyzed asymmetric addition of diethylzinc to aldehydes. *J. Mol. Catal. A Chem.* **2008**, 280, 106–114.

51. Modi, C. K., Solanki, N., Vithalani, R. & Patel, D. Baeyer-Villiger oxidation of cyclopentanone over zeolite Y entrapped transition metal-Schiff base complexes. *Appl. Organomet. Chem.* **2018**, 32, 1–13.

52. Park, S. S. Functionalised mesoporous silica nanoparticles with excellent cytotoxicity against various cancer cells for pH-responsive and controlled drug delivery. *Mater. Des.* **2019**, 184, 108187.

53. Kumaravel, S., Thiripuranthagan, S., Erusappan, E. & Durai, M. Mesoporous Ru/Sn-SBA-15 catalysts: synthesis, characterization and catalytic activity towards hydrogenation of levulinic acid. *J. Porous Mater.* **2022**, 29, 1083–1095.

54. Modi, C. K., Vithalani, R. S., Patel, D. S., Som, N. N. & Jha, P. K. Zeolite-Y entrapped metallo-pyrazolone complexes as heterogeneous catalysts: Synthesis, catalytic aptitude and computational investigation. *Microporous Mesoporous Mater.* **2018**, 261, 275–285.